Biosensors and Bioelectronics 140 (2019) 111341

Contents lists available at ScienceDirect

Biosensors and Bioelectronics

journal homepage: www.elsevier.com/locate/bios

Translating from lab-use to household: Dual-functional upconversion nanoprobes for solar-powered photothermal fluorosis diagnosis

Yuxin Liu, Zheng Wei, Jing Zhou*

Department of Chemistry, Capital Normal University, Beijing, 100048, China

ARTICLE INFO

Keywords:
Photothermal
Upconversion
Fluorosis
Detection
Household

ABSTRACT

Due to the serious symptoms of brittle bones and endocrine disorders, the common disease fluorosis diminishes quality of life. With the aim of developing probes for both laboratory and household fluorosis diagnosis, in this study we rationally designed a novel dual-functional gallic acid-Fe(III) complex-modified upconversion nanoprobe (DF-UCNP) with simultaneous upconversion luminescence (UCL) and photothermal (PT) conversion capacities. The nanoprobe was feasible for UCL fluorine (F^-) detection with a low detection limit of ~20 nM and a broad linear range of 0–50 μM, as well as UCL fluorosis diagnosis both *in vitro* and *in vivo* for lab-use. Furthermore, by utilizing gathered solar irradiation as a PT excitation source and a digital thermometer as a signal reader, the nanoprobe possessed outstanding PT detection capacities for F^- with a detection limit of ~100 nM. Based on this nanoprobe and an accessional self-developed Android application, a household PT kit for fluorosis diagnosis was also constructed. This work provides a new method for rapid laboratory fluorosis diagnosis without a cumbersome determination process as well as household fluorosis diagnosis without requiring specific instruments.

1. Introduction

Fluorosis, a common disease caused by an elevated fluorine (F^-) concentration in living systems, has a significant negative influence on human health due to brittle bones and endocrine disorders(Wei et al., 2018; Zuo et al., 2018). Therefore, it is essential to achieve a highly efficient technique for the diagnosis of fluorosis. Typically, molecular imaging techniques, including magnetic resonance imaging (MRI) and computed tomography (CT), are necessary for a precise diagnosis of fluorosis *via* bone mineral density (BMD) examination(Inês Meurer et al., 2015; Ismail and Hasson, 2008). However, the cumbersome BMD examination process has resulted in these imaging techniques being unaffordable for regular diagnosis. Previous reports demonstrated that serum F^- concentration is a potential fluorosis indicator, which is applicable for regular diagnosis by easy-to-use probes(Jain, 2017). Rare-earth-based upconversion nanophosphors (UCNP) are advanced luminescent probes for biosensing due to their outstanding stability, low toxicity, and ultra-high signal-to-noise luminescence(Dong et al., 2015; Lyu et al., 2018; Wang et al., 2017, 2018; Zhou et al., 2012). Following functionalization of F^--responsive energy acceptors, the upconversion luminescence (UCL) of UCNP is quenched by Förster resonance energy transfer (FRET), and recovered by the addition of F^-, which allows the UCL detection of F^-(Gu and Zhang, 2018; Li et al., 2018; Liu et al., 2017b, 2018d, 2019; Wu et al., 2016; Zhang et al., 2019b; Zhou et al., 2018). With a focus on the accurate determination of serum F^- concentrations, various upconversion nanoprobes have been developed, which has allowed the diagnosis of fluorosis in the laboratory(Liu et al., 2017c, 2018c).

Although many of these probes were developed for luminescence determination of serum F^- concentration, they were unsuitable for household application as the accurate luminescence signal collected required specialized instruments such as a luminescence spectrometer. Recent advance demonstrated that the photothermal (PT) conversion probes are feasible for PT determination of biomolecules by constructing the connection between biomolecule concentration and temperature change under NIR laser irradiation. The PT determination method took the advantage of high sensitivity and low limit of detection due to reduced background noise, which made it applicable in accurate determination of various biomolecules(del Rosal et al., 2016; Zhu et al., 2018). Furthermore, unlike optical signals, temperature can be precisely assessed using a medical thermometer, a common household medical instrument(Fu et al., 2018; Guo et al., 2017; Shu et al., 2017; Zhang et al., 2019a). More importantly, by utilizing the solar as natural NIR resource, specialized NIR laser device was also non-essential for the excitation of PT determination, which further ensured the potential of PT determination in household applications. Therefore, the

* Corresponding author.
E-mail address: jingzhou@cnu.edu.cn (J. Zhou).

https://doi.org/10.1016/j.bios.2019.111341
Received 1 April 2019; Received in revised form 7 May 2019; Accepted 20 May 2019
Available online 23 May 2019
0956-5663/

rational development of a nanoprobe with PT F^- detection capacities is potentially interesting for constructing household PT kit for fluorosis diagnosis.

Compared with other photothermal conversion agents, the gallic acid-Fe(III) complex, one of the main constituent of traditional inks, is a stable and biocompatible F^--responsive energy acceptor and PT conversion agent(An et al., 2018; Jin et al., 2017; Liu et al., 2017a; Zeng et al., 2016). With the addition of F^-, the structure of the gallic acid-Fe (III) complex is destroyed by the strong coordination effect of F^- to the ferric center, which causes a reduction of the near-infrared (NIR) molar extinction coefficient, further weakening the FRET effect and PT conversion. Therefore, gallic acid-Fe(III) complex-modified UCNP may be capable of laboratory UCL determination of serum F^- concentrations and fluorosis diagnosis, as well as household solar-powered PT fluorosis diagnosis utilizing solar NIR irradiation as an excitation source.

Herein, a biocompatible dual-functional gallic acid-Fe(III) complex-modified $NaLuF_4$:Yb,Er@$NaLuF_4$ upconversion nanoprobe (DF-UCNP) was rationally designed for fluorosis diagnosis at both the laboratory and household levels. As the structure of modified gallic acid-Fe(III) complex can be destroyed by F^-, the NIR absorbance intensity of the nanoprobe decreases in response to F^- concentration, which allows for UCL and PT determination. The laboratory-level UCL fluorosis diagnosis was achieved both *in vitro* and *in vivo* using the as-designed nanoprobe. Furthermore, based on this as-designed nanoprobe and an accessional self-developed Android application, a household solar-powered PT kit was also constructed. The household PT fluorosis diagnosis by determining fluorine concentration in various biofluids was also successfully achieved (Fig. 1A).

2. Experimental section

2.1. Preparation of DF-UCNP

The core-shell $NaLuF_4$:Yb,Er@$NaLuF_4$ upconversion nanoparticles (UCNP) were prepared *via* a typical solvothermal method(Liu et al., 2016). The hydrophilic transfer and gallic acid-Fe(III) complex modification of UCNP was performed based on a ligand exchange protocol (Liu et al., 2017d, 2018b). Please see the Supporting Information for experimental details.

2.2. UCL and PT F^- detection capacities

The F^- solution was prepared by dissolving NaF in DI water and adjusted to neutral by diluted HCl solution. F^- solutions with various concentrations (0–50 μM) were added into DF-UCNP suspensions (2 mg mL^{-1}) and incubated for 5 min. To study the selectivity of DF-UCNP for F^- detection, various ions and biomolecules (5 mM) were added into DF-UCNP suspension (2 mg mL^{-1}). Then, the UCL spectra were measured and the photothermal (PT) detection was performed using a thermocouple under 808 nm laser irradiation (1.5 W cm^{-2}) for 240 s, respectively. The limit of detection (LOD) was determined according to previously reported standardized approach (Taleuzzaman,

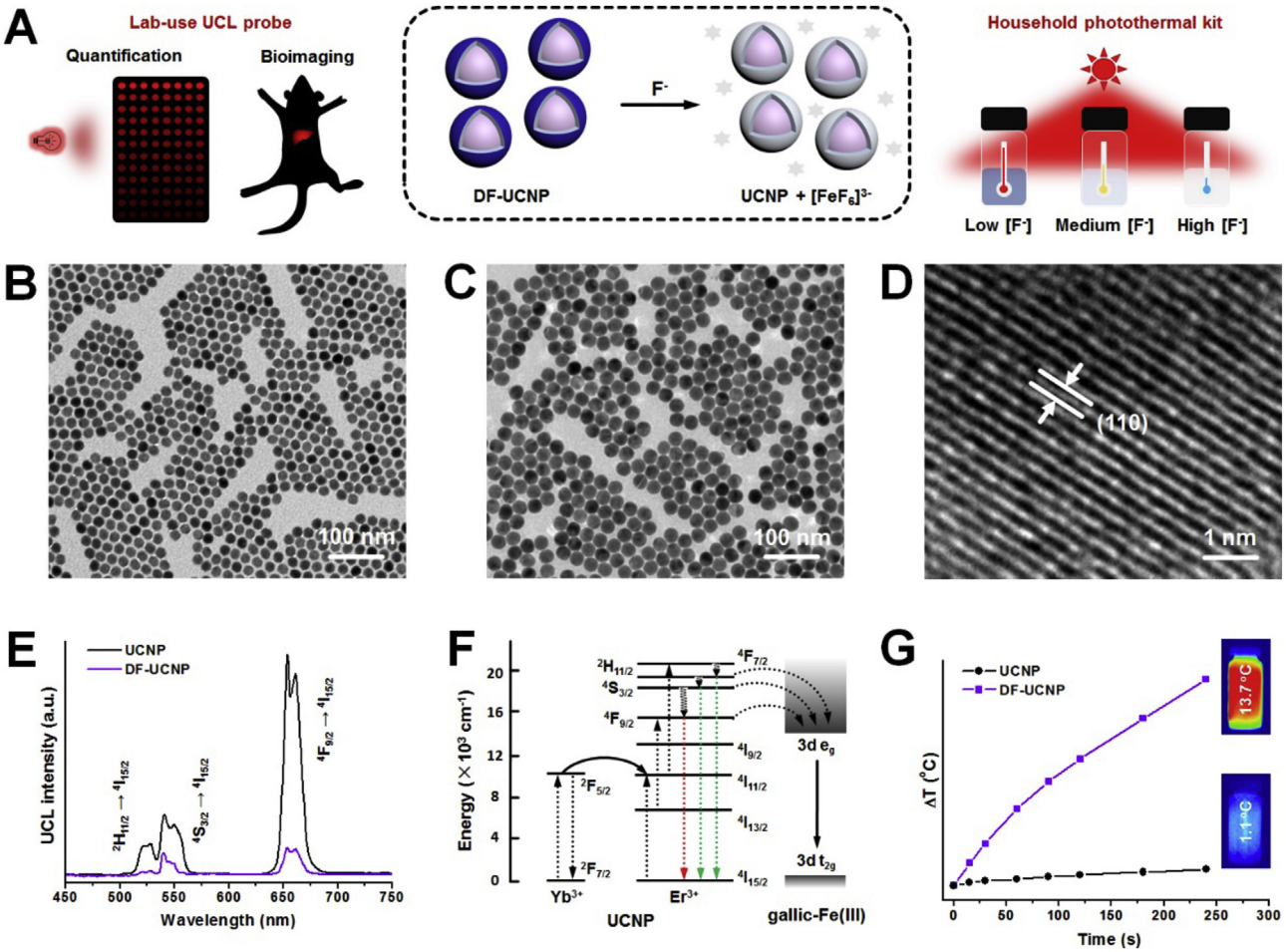

Fig. 1. Preparation and characteristics of the DF-UCNP. (A) Proposed mechanism for F^- detection of DF-UCNP and fluorosis diagnosis application in laboratory and in house. TEM images of $NaLuF_4$:Yb,Er (B) and $NaLuF_4$:Yb,Er@$NaLuF_4$ (UCNP) (C) prepared *via* a typical solvothermal method. (D) HR-TEM image of UCNP. (E) UCL spectra of UCNP and DF-UCNP. (F) Proposed mechanism of energy transfer between UCNP and the modified gallic acid-Fe(III) complex. (G) ΔT curve of UCNP and DF-UCNP under 808 nm irradiation within 4 min. Data are represented as mean ± RSD.

2018).

2.3. Lab-use UCL serum F^- concentration monitoring and imaging

All animal procedures were performed in accordance with the Guidelines for Care and Use of Laboratory Animals of Beijing Vital River Laboratory Animal Technology Co., Ltd. and approved by the Animal Ethics Committee of the Vital River Institutional Animal Care and Use Committee (VR IACUC). Hepatocyte (CCC-HEL-1) cells were provided by the Institute of Basic Medical Sciences of the Chinese Academy of Medical Sciences. The blood half-life of DF-UCNP was calculated by the model of first-order elimination kinetics. Fluorosis mice model was established according to our previous works(Liu et al., 2018c). Fluorosis mice receiving calcium chloride intravenous injection (4 mg kg^{-1}) was used for comparison. UCL imaging and signal analysis of mice were performed 4 h after DF-UCNP intravenous injection (10 mg kg^{-1}). Please see the Supporting Information for experimental details.

2.4. Household solar-powered PT kit

The kit contained needles (amicrobic), sampling tubes (amicrobic, 200 μL), working solutions (2 mg mL^{-1} DF-UCNP suspension), reference solutions (2 mg mL^{-1} DF-UCNP suspension containing 0, 10, 20, 30, 40, and 50 μM F^-), and a digital thermometer. Furthermore, a fixator including a concave mirror was also provided for effective concentration of sunlight. In a typical experiment to correct the PT calibration curve, sunlight was gathered by the concave mirror and the reference solutions were settled at the focal point. The temperatures of the reference solutions were then read by the digital thermometer within 240 s. The experiments were performed in a closed room with an air conditioner. The average surrounding temperature was measured and calculated by the digital readout of four thermocouples that were settled near the fixator. The average surrounding temperature on sunny days and cloudy days for fluorosis diagnosis by Android APP was 23.4 °C and 27.5 °C, respectively. For sample determination, 200 μL of liquid sample was collected from the sampling tubes and mixed with the working solution, incubated for 5 min at room temperature, and determined as above. A statistical analysis was performed according to previous reports(Brunelle et al., 2017; Huynh et al., 2015).

3. Results and discussion

3.1. Preparation and characterization of DF-UCNP

Using a typical solvothermal method, uniform core-shell $NaLuF_4$:Yb,Er@$NaLuF_4$ upconversion nanoparticles (UCNP) were prepared. Transmission electron microscopy (TEM) images showed that $NaLuF_4$:Yb,Er was almost spherical in shape with an average diameter of 15.15 ± 1.70 nm, while the size of the UCNP increased to 23.31 ± 2.11 nm, which suggested that the $NaLuF_4$ inner shell was successfully coated on $NaLuF_4$:Yb,Er (Fig. 1B,C and Fig. S1). Importantly, the upconversion luminescence (UCL) was significantly enhanced after the coating with the $NaLuF_4$ shell, contributing to the inhibition of multiphonon relaxation between emitters and absorbed ligands (Fig. S2). Furthermore, high-resolution TEM (HR-TEM) images and X-ray diffraction (XRD) patterns suggested that the UCNP had a defined (110) crystallographic plane, corresponding to the standard card of high crystallized hexagonal phase $NaLuF_4$ (JCPDS: 027–0726, Fig. 1D and Fig. S3).

To endow the UCNP with F^--responsive capacities, the gallic acid-Fe(III) complex was then modified *via* a ligand-exchange protocol (DF-UCNP). TEM image suggested that the modification of gallic acid-Fe(III) complex hardly influence the morphology of UCNP (Fig. S4). Both ultraviolet–visible–near infrared (UV–vis–NIR) spectra and Föurier transmission infrared (FTIR) spectra confirmed the successful modification of gallic acid-Fe(III) (Figs. S5 and 6). The modified gallic acid-Fe(III) had strong absorbance in the red and NIR spectral region, which was attributed to the d-d transition of Fe(III) influenced by gallic acid ligands(Liu et al., 2018a; Yan et al., 2018). Therefore, an energy transfer may occur between UCNP and modified gallic acid-Fe(III), resulting in significant quenching of red UCL (654 nm, $^4F_{9/2} \rightarrow {}^4I_{15/2}$) (Fig. 1E and F). Moreover, the DF-UCNP was feasible for photothermal (PT) conversion under 808 nm laser irradiation, increasing the surrounding temperature by 13.7°C within 240 s (Fig. 1G). The DF-UCNP also had outstanding dispersibility and photostability in various conditions (Fig. S7). More importantly, the gallic acid-Fe(III) complex modified on UCNP had better photostability and storage stability than their monomers, which not only highlighted the essential role of UCNP as carrier but also made them much more feasible for actual applications (Fig. S8). The above results demonstrated that DF-UCNP had been successfully developed with outstanding UCL and PT conversion capacities.

3.2. UCL and PT detection of F^- by DF-UCNP

As the modified gallic acid-Fe(III) complex was destroyed, the Förster resonance energy transfer (FRET) between UCNP and gallic acid-Fe(III) was reduced after the addition of F^-, which was confirmed by the prolonged luminescence lifetime (Fig. 2A). Therefore, UCL intensity of DF-UCNP was recovered in the presence of F^-. With increased F^- concentration ($[F^-]$), the UCL in both the green and red spectral region increased accordingly (Fig. 2B). It should noted that the red-to-green UCL ratio of DF-UCNP also increased as $[F^-]$ increased, and showed a positive curve relationship with $[F^-]$ at 0–50 μM (I_{654}/I_{540} = 3.798–2.864 exp (-0.046 $[F^-]$/μM); R^2 = 0.9965, LOD: 5 nM, Fig. 2C), which allowed DF-UCNP to be a ratiometric UCL probe for F^- detection.

When F^- was added, the absorbance of DF-UCNP in the red and NIR spectral region decreased due to destruction of the gallic acid-Fe(III) complex and formation of colorless $[FeF_6]^{2-}$ ions (Fig. 2D). Correspondingly, the PT conversion effect of DF-UCNP was reduced with increased $[F^-]$ (Fig. 2E). In the $[F^-]$ range of 0–50 μM, the temperature change (ΔT) of DF-UCNP within 240 s of receiving 808 nm laser irradiation showed a positive linear relationship with $[F^-]$ (ΔT/°C = 13.513–0.208 $[F^-]$/μM; R^2 = 0.9989, LOD: 100 nM, Fig. 2F). Importantly, the irradiation time did not affect the linear correlation, which made it much easier for household applications (Fig. S9).

Furthermore, typical ions and biomolecules with relatively strong coordination in plasma had no obvious influence on the UCL and PT conversion capacities of DF-UCNP, which illustrated that DF-UCNP had good selectivity for F^- (Fig. 2G,H and Fig. S10). Compare with previous works, the UCL method had comparable detection capacities, while the PT method had the advantage that required no expensive and specialize instruments (Table S1). Based on the above findings, DF-UCNP was applicable to the detection of F^- by either the UCL or PT method, and had potential in fluorosis diagnosis.

3.3. Laboratory fluorosis diagnosis and UCL ratiometric imaging

As UCNPs have outstanding stability and gallic acid-Fe(III) is the main constituent of traditional inks, DF-UCNP was safe for bioapplications, a conclusion supported by the negative cytotoxicity and good biocompatibility results (Fig. S11).(Gnach et al., 2015; Zeng et al., 2016) As UCL is applicable for accurate determination and bioimaging, DF-UCNP was assessed for the laboratory diagnosis of fluorosis in terms of both serum F^- concentration monitoring *in vitro* and UCL ratiometric imaging *in vivo*. A fluorosis mouse model was established using a typical protocol based on our previous reports(Liu et al., 2018c). The serum and urine F^- concentrations in mice with fluorosis were determined by the UCL method using DF-UCNP and were found to be significantly higher than those in normal mice (Fig. S12A). More importantly, the

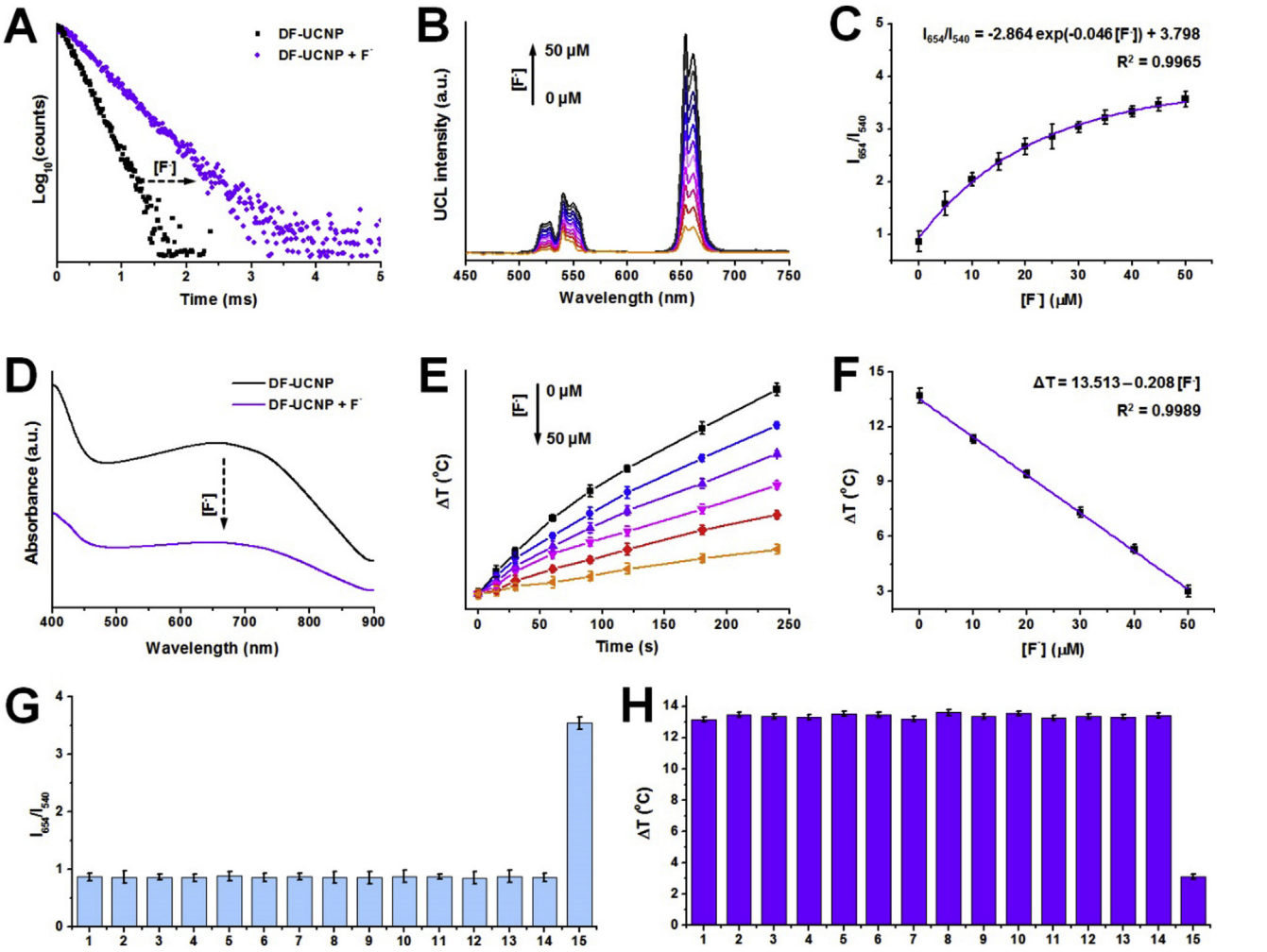

Fig. 2. F^- detection capacities of the DF-UCNP. (A) Luminescence lifetime of DF-UCNP in the absence and presence of F^-. (B) UCL spectra of DF-UCNP reacted with various [F^-]. (C) The linear relationship between F^- concentration and I_{654}/I_{540} in the range of 0–50 μM. (D) UV–vis–NIR spectra of DF-UCNP in the absence and presence of F^-. (E) ΔT curve of DF-UCNP reacted with various [F^-]. (F) The linear relationship between [F^-] and ΔT in the range of 0–50 μM. UCL I_{654}/I_{540} response (G) and ΔT response (H) of DF-UCNP in the presence containing typical biomolecules in plasma with relative strong coordination ability: 1. BSA; 2. HSA; 3. Fibrin; 4. Methionine; 5. Arginine; 6. Cystine; 7. Cysteine; 8. Homocysteine; 9. GSH; 10. GSSG; 11. Glucose; 12. Pyruvic acid; 13. Gluconic acid; 14. 2-Hydroxypropanoic acid; 15. F^-. Data are represented as mean ± RSD.

serum F^- concentration decreased after the intravenous administration of calcium chloride, a typical fluorosis drug, suggesting that DF-UCNP could be used to evaluate the therapeutic effect of medicines used in the treatment of fluorosis (Fig. S12B).

Therefore, further studies on ratiometric UCL imaging in mice with fluorosis were carried out to evaluate the performance of DF-UCNP in fluorosis diagnosis *in vivo*. Due to its good dispersibility and small hydrodiameter, DF-UCNP had a prolonged blood circulation half-life time (~4.72 h, Fig. S12C and Fig. S13). After intravenous injection, DF-UCNP circulated in the vessels and captured F^- in the blood, finally accumulating in reticuloendothelial system of mice, such as the liver. Following intravenous injection of DF-UCNP, both the red UCL signal (*Abbr.* as R, 650 ± 15 nm) and the green UCL signal (*Abbr.* as G, 400–600 nm) in mice with fluorosis were significantly higher than those in normal mice, reflecting the higher serum F^- concentrations in mice with fluorosis compared with normal mice (Figs. S12D and E). The R/G ratiometric images further confirmed this finding. Mice with fluorosis had a higher R/G ratio than normal mice, which demonstrated that DF-UCNP reacted with F^- resulting in the identification of differences in serum F^- concentration between the mice with fluorosis and normal mice. To evaluate the feasibility of DF-UCNP in fluorosis diagnosis, the UCL signal was counted and the R/G ratio was calculated. The UCL intensity and R/G ratio in mice with fluorosis were significantly higher than those in normal mice, which suggested that UCL ratiometric imaging by DF-UCNP was feasible for fluorosis diagnosis *in vivo* (Fig. S12F). Though the [F^-] in blood couldn't be precisely calculated by the R/G ratio due to the different scattering and absorbing efficiency of tissues to UCL at various wavelengths, the R/G ratio was applicable to exhibit the serum F^- level semi-quantificationally, further allowing fluorosis diagnosis by UCL imaging *in vivo* (Fig. S12G). These results strongly suggested that DF-UCNP is applicable for the laboratory determination of serum F^- concentration and fluorosis diagnosis by UCL ratiometric imaging.

3.4. Household solar-powered PT fluorosis diagnosis

While the UCL method was useful for laboratory fluorosis diagnosis, the PT method possessed great potential for application in household fluorosis diagnosis. By utilizing the PT F^- detection capacity of DF-UCNP, a household PT kit was developed using a common digital thermometer for signal reading (Fig. 3A). As solar radiation is a natural NIR-emitting resource that is widely available, the kit was powered by gathered solar irradiation instead of a NIR laser (Fig. 3B). The power density of the gathered solar irradiation reached ~1.98 W cm^{-2} on a

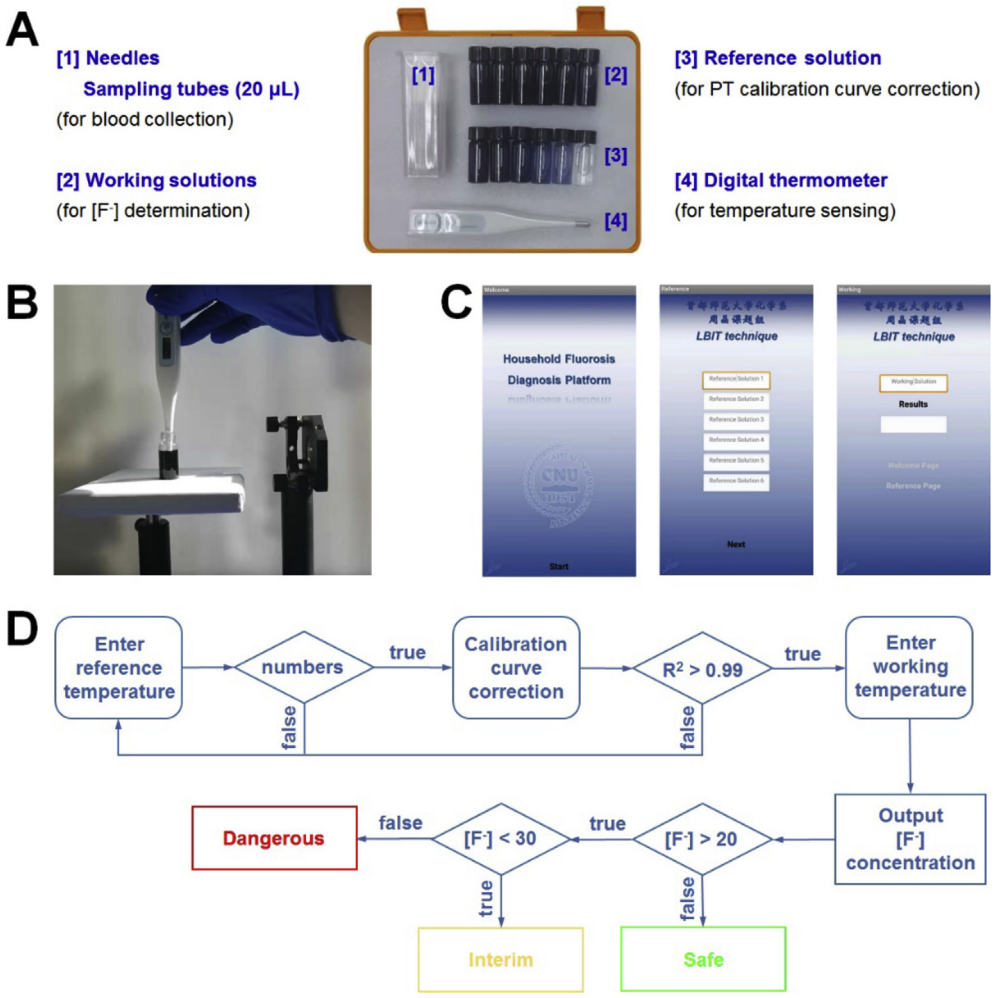

Fig. 3. Household solar-powered PT kit and accessional Android APP. The digital photograph of household solar-powered fluorosis diagnosis kit (A) and fixator (B). The work solution was the DF-UCNP solution for F^- detection. The reference solution was the DF-UCNP solution containing various [F^-] (0, 10, 20, 30, 40, and 50 μM). The printscreen (C) and the logical operation route (D) of the self-developed accessional Android APP.

typical sunny day, and the power density on cloudy days was still higher than 0.5 W cm^{-2}, which was applicable for activating the PT conversion of DF-UCNP (Figs. S14A and C). To correct the calibration curve for PT detection, a series of DF-UCNP reference solutions containing various [F^-] were prepared for the kit. By determining the temperature of reference solutions under gathered solar irradiation within 240 s, the PT calibration curves for F^- detection on the studied sunny day and cloudy day were obtained. The ΔT was linearly related to [F^-] on both the sunny day ($\Delta T/^oC = 15.666–0.237\ [F^-]/\mu M$; $R^2 = 0.9994$, Fig. S14B) and the cloudy day ($\Delta T/^oC = 6.719–0.096\ [F^-]/\mu M$; $R^2 = 0.9996$, Fig. S14D) in the [F^-] range of 0–50 μM, although the slope of the curve on the sunny day was higher than that on the cloudy day. It was also found that the environmental temperature had no obvious effect on the linear relationship between ΔT and [F^-] (Fig. S15).

To simplify the process of data analyzing and diagnosing, an accessional Android application (APP) named household fluorosis diagnosis (HFD) platform was developed by our group. The welcome page of HFD platform analyzer contained only one functional buttons of "Start", which could reset all the inputted data and determination records (Fig. 3C). On the reference page, the calibration curve could be established by entering temperature of reference solution respectively and tapping the "Next" functional button. If the coefficient of determination (R^2) was higher than 0.99, the page will redirect to the working page (Fig. 3D). When the temperature of working solution was inputted, the "Results" functional button would allow the output of [F^-]. According to previous reports, the [F^-] in normal body fluids should be lower than 20 μM, while fluorosis cases had higher fluids [F^-] than 30 μM. Therefore, a logical operation was also added to evaluate the level of fluorosis risk. The [F^-] that lower than 20 μM was identified to the "Safe" grade and that high than 30 μM was "Dangerous" grade, which provided the basic index for fluorosis diagnosis (Fig. 4A). Furthermore, the cases that had [F^-] in the middle of 20 and 30 μM was classified to be interim, which was potentially in the risk of fluorosis. Therefore, the solar-powered PT kit with an accessional Android APP was successfully constructed.

To ensure the applicability of household fluorosis diagnosis by the as-developed solar-powered PT kit, accurate temperature determination and protocol precision were essential and should be guaranteed. The accuracy of temperature determination by digital thermometer was studied using lab-use thermoelectric couple as standard reference (Fig. 4B). It was found that temperature determined by digital thermometer was in accordance with that by accurate lab-use thermoelectric couple. Moreover, the accuracy of serum [F^-] determination by solar-powered PT method was evaluated using standard colorimetric protocol (GB 7483–1987) and electrochemical method as comparison (Fig. 4C and Fig. S16). It was found that serum [F^-] determined by the PT method was in accordance with both the colorimetric and electrochemical method, which suggested that the PT method was feasible for accurate serum [F^-] determination. Furthermore, the accuracy of

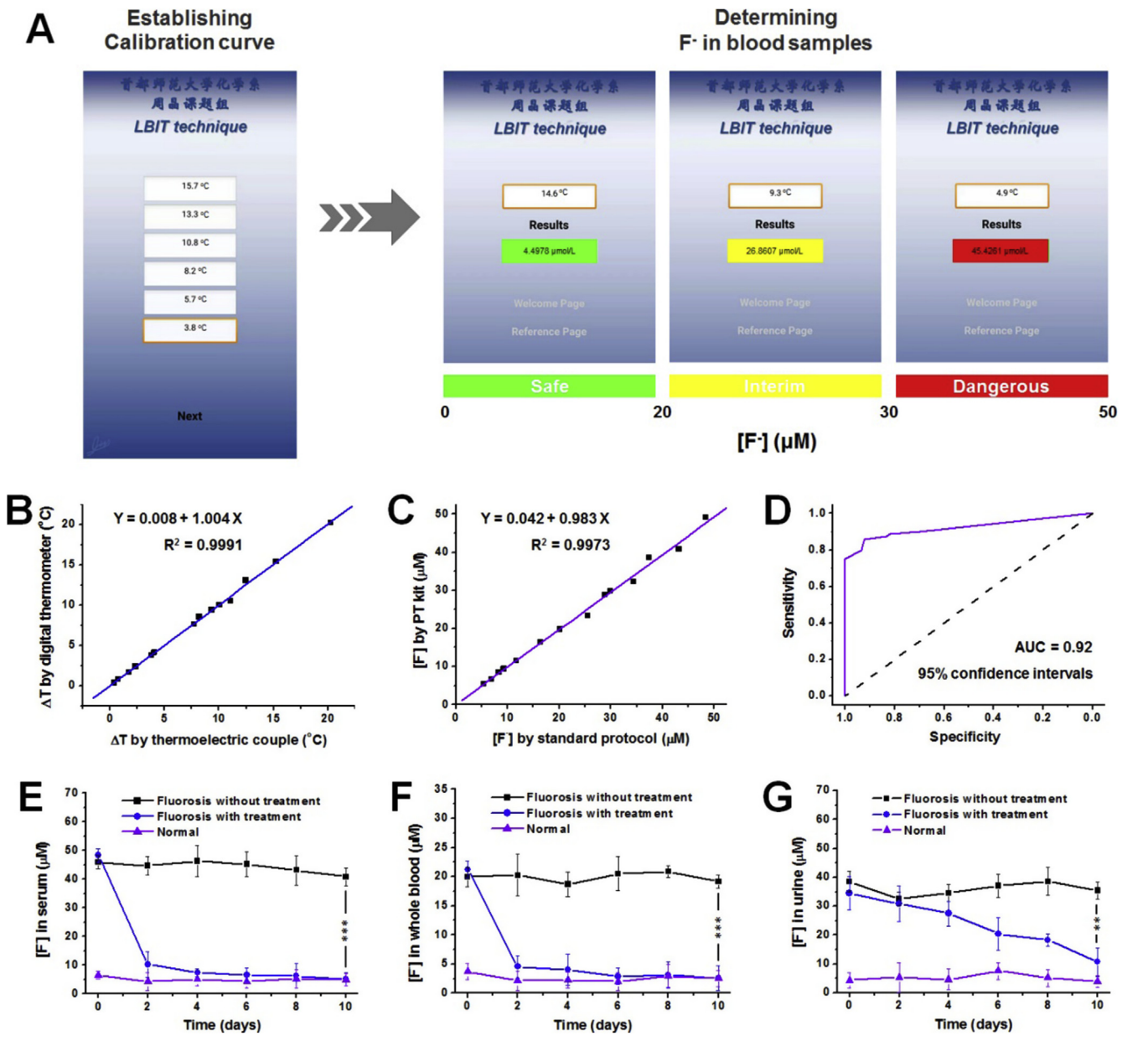

Fig. 4. Fluorosis diagnosis by household solar-powered PT kit. (A) The printscreen of accessional Android APP in the process of [F^-] determination and fluorosis diagnosis. (B) Linear correlation between temperatures determined by digital thermometer and by thermoelectric couple. (C) Linear correlation between readout results from APP and by standard colorimetric protocol. (D) Receiver operating characteristic (ROC) curve presenting the probability for the assay to correctly distinguish between normal and fluorosis cases based on the serum [F^-] in the blood samples determined by PT method. Random choice is denoted by the black dotted diagonal line. [F^-] in serum (E), blood (F), and urine (G) of fluorosis and normal mice throughout the treatment process. Data are represented as mean ± RSD.

fluorosis diagnosis *via* serum [F^-] determination using the household solar-powered PT kit was demonstrated by the receiver operating characteristic (ROC) analysis (Fig. 4D). The area under the curve (AUC) generated for the fluorosis cases was estimated to be 0.92 (95% confidence intervals) from the ROC curve, indicating that there was a 92% chance of correctly identifying fluorosis using the household solar-powered PT kit. Therefore, the household fluorosis diagnosis based on the solar-powered PT kit was reliable. To further demonstrate the serum F^- level determination and fluorosis diagnosis capacities of the solar-powered PT method, three typical indexes were determined within a 10 days period of calcium chloride treatment, namely, the F^- level in serum, blood, and urine. Within the therapeutic period, the [F^-] in all three body fluids that collected from fluorosis mice receiving treatment continuously decreased and practically returned to normal, while that of those mice receiving no treatment remained high and showed a significant difference to those receiving treatment, which demonstrated that the solar-powered PT method could accurately monitor the change of [F^-] in various fluids within treatment period and diagnose the fluorosis (Fig. 4E–G). The above results demonstrated that the PT kit could not only identify the fluorosis cases, but be able to evaluate the severity of fluorosis within the therapeutic process. Therefore, the solar-powered PT kit was applicable for household F^- detection, as well as [F^-] determination and fluorosis diagnosis.

4. Conclusion

In this study, a dual-functional gallic acid-Fe(III) complex-modified $NaLuF_4$:Yb,Er@$NaLuF_4$ upconversion nanoprobe (DF-UCNP) was

developed for UCL and PT dual-model F^- detection, serum [F^-] determination, and fluorosis diagnosis. Both the UCL and PT methods had a low limit of detection (5 nM for the UCL method and 100 nM for the PT method), a broad linear range (0–50 μM), and high selectivity for F^-. The as-developed DF-UCNP was feasible for UCL determination of serum [F^-] and F^- imaging *in vivo*, and for laboratory diagnosis of fluorosis. Importantly, by utilizing the PT detection capacities of F^- and an accessional self-developed Android APP, a household solar-powered PT kit was constructed for fluorosis diagnosis. The kit possessed high accuracy for serum [F^-] determination and fluorosis diagnosis under various conditions. Our results not only provide a novel insight into the development of a nanoprobe for both laboratory and household bioapplications, but also highlight the potential of the PT method for constructing household determination kits.

Declaration of interests

The authors declare that they have no known competing financial interests or personal relationships that could have appeared to influence the work reported in this paper.

CRediT authorship contribution statement

Yuxin Liu: Conceptualization, Data curation, Formal analysis, Investigation, Methodology, Project administration, Resources, Software, Validation, Visualization, Writing - original draft, Writing - review & editing. **Zheng Wei:** Data curation, Formal analysis, Investigation, Methodology, Resources, Validation, Visualization, Writing - original draft, Writing - review & editing. **Jing Zhou:** Conceptualization, Funding acquisition, Methodology, Project administration, Resources, Supervision, Validation, Writing - original draft, Writing - review & editing.

Acknowledgement

The authors thank the funding of Beijing Talent Foundation Outstanding Young Individual Project (2015000026833ZK02), Beijing Municipal Education Commission Outstanding Young Individual Project (CIT&TCD201904082), The Joint Foundation Program of Beijing Municipal Natural Science Foundation and Beijing Municipal Education Commission (KZ201810028045), Capacity Building for Sci-Tech Innovation-Fundamental Scientific Research Funds (19530050179), Project of High-level Teachers in Beijing Municipal Universities in the Period of 13th Five-year Plan (IDHT20180517), Project of Construction of Scientific Research Base by the Beijing Municipal Education Commission, Yanjing Young Scholar Program of Capital Normal University, and Youth innovative research team of Capital Normal University.

Appendix A. Supplementary data

Supplementary data to this article can be found online at https://doi.org/10.1016/j.bios.2019.111341.

References

An, L., Yan, C., Mu, X., Tao, C., Tian, Q., Lin, J., Yang, S., 2018. ACS Appl. Mater. Interfaces 10, 28483–28493.
Brunelle, E., Le, A.M., Huynh, C., Wingfield, K., Halámková, L., Agudelo, J., Halámek, J., 2017. Anal. Chem. 89, 4314–4319.
del Rosal, B., Carrasco, E., Ren, F., Benayas, A., Vetrone, F., Sanz-Rodríguez, F., Ma, D., Juarranz, Á., Jaque, D., 2016. Adv. Funct. Mater. 26, 6060–6068.
Dong, H., Du, S.-R., Zheng, X.-Y., Lyu, G.-M., Sun, L.-D., Li, L.-D., Zhang, P.-Z., Zhang, C., Yan, C.-H., 2015. Chem. Rev. 115, 10725–10815.
Fu, G., Sanjay, S.T., Zhou, W., Brekken, R.A., Kirken, R.A., Li, X., 2018. Anal. Chem. 90, 5930–5937.
Gnach, A., Lipinski, T., Bednarkiewicz, A., Rybka, J., Capobianco, J.A., 2015. Chem. Soc. Rev. 44, 1561–1584.
Gu, B., Zhang, Q., 2018. Adv. Sci. 5, 1700609.
Guo, Q., Liu, Y., Jia, Q., Zhang, G., Fan, H., Liu, L., Zhou, J., 2017. Anal. Chem. 89, 4986–4993.
Huynh, C., Brunelle, E., Halámková, L., Agudelo, J., Halámek, J., 2015. Anal. Chem. 87, 11531–11536.
Inês Meurer, M., Caffery, L.J., Bradford, N.K., Smith, A.C., 2015. J. Telemed. Telecare 21, 449–458.
Ismail, A.I., Hasson, H., 2008. J. Am. Dent. Assoc. 139, 1457–1468.
Jain, R.B., 2017. Environ. Toxicol. Pharmacol. 50, 20–31.
Jin, Q., Zhu, W., Jiang, D., Zhang, R., Kutyreff, C.J., Engle, J.W., Huang, P., Cai, W., Liu, Z., Cheng, L., 2017. Nanoscale 9, 12609–12617.
Li, Z., Yuan, H., Yuan, W., Su, Q., Li, F., 2018. Coord. Chem. Rev. 354, 155–168.
Liu, T., Zhang, M., Liu, W., Zeng, X., Song, X., Yang, X., Zhang, X., Feng, J., 2018a. ACS Nano 12, 3917–3927.
Liu, Y., Fan, H., Guo, Q., Jiang, A., Du, X., Zhou, J., 2017a. Theranostics 7, 4217–4228.
Liu, Y., Guo, Q., Zhu, X., Feng, W., Wang, L., Ma, L., Zhang, G., Zhou, J., Li, F., 2016. Adv. Funct. Mater. 26, 5120–5130.
Liu, Y., Jia, Q., Guo, Q., Jiang, A., Zhou, J., 2017b. Anal. Chem. 89, 12299–12305.
Liu, Y., Jia, Q., Guo, Q., Wei, W., Zhou, J., 2018b. Biomaterials 180, 104–116.
Liu, Y., Jia, Q., Zhai, X., Mao, F., Jiang, A., Zhou, J., 2019. Chem. Sci. 10, 1193–1200.
Liu, Y., Jiang, A., Jia, Q., Zhai, X., Liu, L., Ma, L., Zhou, J., 2018c. Chem. Sci. 9, 5242–5251.
Liu, Y., Ouyang, Q., Li, H., Zhang, Z., Chen, Q., 2017c. ACS Appl. Mater. Interfaces 9, 18314–18321.
Liu, Y., Tu, D., Zheng, W., Lu, L., You, W., Zhou, S., Huang, P., Li, R., Chen, X., 2018d. Nano Res 11, 3164–3174.
Liu, Y., Zhang, G., Guo, Q., Ma, L., Jia, Q., Liu, L., Zhou, J., 2017d. Biomaterials 112, 204–217.
Lyu, L., Cheong, H., Ai, X., Zhang, W., Li, J., Yang, H., Lin, J., Xing, B., 2018. NPG Asia Mater. 10, 685–702.
Shu, B., Zhang, C., Xing, D., 2017. Biosens. Bioelectron. 97, 360–368.
Taleuzzaman, M., 2018. Organ. Med. Chem. Int. J. 7, 555722.
Wang, D., Wei, W., Singh, A., He, G.S., Kannan, R., Tan, L.-S., Chen, G., Prasad, P.N., Xia, J., 2017. ACS Photonics 4, 2699–2705.
Wang, Y., Zheng, K., Song, S., Fan, D., Zhang, H., Liu, X., 2018. Chem. Soc. Rev. 47, 6473–6485.
Wei, Y., Zeng, B., Zhang, H., Chen, C., Wu, Y., Wang, N., Wu, Y., Zhao, D., Zhao, Y., Iqbal, J., Shen, L., 2018. Toxicol. Lett. 291, 39–50.
Wu, Y.-X., Zhang, X.-B., Zhang, D.-L., Zhang, C.-C., Li, J.-B., Wu, Y., Song, Z.-L., Yu, R.-Q., Tan, W., 2016. Anal. Chem. 88, 1639–1646.
Yan, Q., Chen, Z.-H., Xue, S.-F., Han, X.-Y., Lin, Z.-Y., Zhang, S., Shi, G., Zhang, M., 2018. Sensor. Actuator. B Chem. 268, 108–114.
Zeng, J., Cheng, M., Wang, Y., Wen, L., Chen, L., Li, Z., Wu, Y., Gao, M., Chai, Z., 2016. Adv. Healthc. Mater. 5, 772–780.
Zhang, D., Du, S., Su, S., Wang, Y., Zhang, H., 2019a. Biosens. Bioelectron. 123, 19–24.
Zhang, Z., Shikha, S., Liu, J., Zhang, J., Mei, Q., Zhang, Y., 2019b. Anal. Chem. 91, 548–568.
Zhou, J., Liu, Z., Li, F., 2012. Chem. Soc. Rev. 41, 1323–1349.
Zhou, L., Fan, Y., Wang, R., Li, X., Fan, L., Zhang, F., 2018. Angew. Chem. Int. Ed. 57, 12824–12829.
Zhu, X., Li, J., Qiu, X., Liu, Y., Feng, W., Li, F., 2018. Nat. Commun. 9, 2176.
Zuo, H., Chen, L., Kong, M., Qiu, L., Lü, P., Wu, P., Yang, Y., Chen, K., 2018. Life Sci. 198, 18–24.